Quantum-control-landscape structure viewed along straight paths through the space of control fields

Arun Nanduri,[1] Tak-San Ho,[2] and Herschel Rabitz[2,*]
[1]*Department of Chemistry, Columbia University, New York, New York 10027, USA*
[2]*Department of Chemistry, Princeton University, Princeton, New Jersey 08544, USA*
(Received 28 December 2015; published 25 February 2016)

The dynamics of closed quantum systems may be manipulated by using an applied field to achieve a control objective value for a physical goal. The functional relationship between the applied field and the objective value forms a quantum control landscape, and the optimization process consists of a guided climb up the landscape from the bottom to the top. Two classes of landscape features are important for understanding the ease of finding an optimal control field. The first class of topological landscape features has been proven to be especially simple in that no suboptimal local maxima exist (upon satisfaction of certain assumptions), which partially accounts for the ease of finding optimal fields. Complementary to the topology, the second class of features entails the landscape structure, characterizing the sinuous nature of the paths leading to an optimal control field. Previous work found that the landscape structure is also particularly simple, as excursions up the landscape guided by a gradient algorithm correspond to nearly straight paths through the space of control fields. In this paper we take an alternative approach to examining landscape structure by constructing, and then following, exactly straight trajectories in control space. Each trajectory starts at a corresponding point on the bottom of the landscape and ends at an associated point on the top, with the observable values taken either as the state-to-state transition probability, the expectation value of a general observable, or the distance from a desired unitary transformation. In some cases the starting point is at a suboptimal critical-point saddle, with the goal, again, of following a straight field path to the optimal objective yield or another suboptimal critical point. We find that the objective value almost always rises monotonically upon following a straight control path from one critical point to another, which shows that landscape structure is very simple, being devoid of rough bumps and gnarled "twists and turns". An analysis reveals that the generally featureless nature of quantum control landscapes can be understood in terms of the occurrence of many interfering quantum pathways contributing while traversing the landscape, essentially smoothing out the terrain. These results also provide a basis for further studies to seek a new efficient algorithm to discover optimal fields by means of taking into account the inherently smooth landscape structure.

DOI: 10.1103/PhysRevA.93.023427

I. INTRODUCTION

Quantum optimal control theory (OCT) [1,2] has provided a foundation for the increasing success of quantum control experiments [3]. Typically, these experiments involve adjusting the form of an applied field under algorithmic guidance to produce the desired system performance. Recent successes include manipulating population dynamics in Bose-Einstein condensates [4], controlling ionization of silver atoms [5], minimizing the defects created in a quantum phase transition [6], and coherently transporting energy in light-harvesting complexes [7], among many other applications. Closed-loop learning algorithms [8] directing pulse shapers [9] have allowed for finding optimal control fields with only modest experimental effort. Theoretical analysis bolstered by simulations [10] attributes the ease of finding effective controls to the nature of the underlying *quantum control landscape* [11], which is the physical observable as a functional of the control field. The present work employs simulations and carries out additional analysis to show that quantum control landscapes appear exceptionally smooth. This finding provides the basis for ultimately creating especially efficient optimal control algorithms.

We consider a closed N-level quantum system driven by a time-dependent field, $E(t), t \in [0,T]$. In the dipole approximation, the system is described by the Hamiltonian

$$H(t) = H_0 - \mu E(t), \tag{1}$$

where H_0 is a diagonal matrix representing the field-free Hamiltonian and μ is the dipole moment matrix. The system evolves according to the unitary matrix $U(t) \equiv U(t;0)$, which satisfies the Schrödinger equation

$$i\hbar \frac{\partial U(t,0)}{\partial t} = H(t)\,U(t,0), \quad U(0,0) = 1. \tag{2}$$

The desired control objective J expressed as a function of the final propagator $U(T)$ specifies a cost functional, $J[E(\cdot)]$, forming a quantum control landscape, which associates a value of J with every control field. In this work we consider either the state-to-state transition probability landscape $J_{if} = P_{i\to f} = |\langle f|U(T)|i\rangle|^2$, the quantum ensemble control landscape $J_O = \mathrm{Tr}\,(\rho(T)O) = \mathrm{Tr}\,(U(T,0)\rho(0)U^\dagger(T,0)O)$, or the unitary transformation landscape $J_W = \|W - U(T)\|^2 = 2N - 2\mathrm{Re}\{\mathrm{Tr}\,(W^\dagger U(T))\}$, relevant for quantum information processing [12]. Here $|i\rangle$ and $|f\rangle$ are eigenstates of H_0, $\rho(0)$ is the initial density matrix of the ensemble, W is a unitary matrix, and $\|\cdot\|$ denotes the Frobenius norm. Starting from an arbitrary control field, one may optimize a particular cost functional J using a suitable algorithm, such as the D-MORPH [13] gradient-based procedure. Using this algorithm, the form of the field will morph along a landscape gradient ascent trajectory, and we conveniently introduce a variable

*hrabitz@princeton.edu

$0 \leqslant s \leqslant s_{\max}$ which parametrizes the control field $E(t) \rightarrow E(s,t)$ to follow its form as a function of t, as s is systematically increased. The goal is to find a field $E(s_{\max},t)$ that produces a high-quality outcome at $s = s_{\max}$ located acceptably close to the optimal value of the landscape. In this fashion an optimization can be viewed as generating a corresponding trajectory through control space, starting from the initial field $E(0,t)$, which yields a low value of J, and then reaching the final field $E(s_{\max},t)$, providing the nearly optimal value of J.

Previous work found that when certain conditions are satisfied, the *topology* of the transition probability control landscape $P_{i\rightarrow f}(T)$ is especially amenable to finding optimal quantum controls, in that all critical points, or control fields $E(t)$ for which $\frac{\delta P_{i\rightarrow f}}{\delta E(t)} = 0 \ \forall t \in [0,T]$, are located at either the bottom or the top of the landscape. In particular, this statement is valid, regardless of whether or not the quantum system of interest is degenerate, whenever the following three basic assumptions are satisfied: (i) the quantum system is controllable, (ii) the functional derivatives $\frac{\delta U_{ij}(T)}{\delta E(t)} \ \forall i,j$ are linearly independent functions of time $t \in [0,T]$, and (iii) the controls are not constrained. Upon the satisfaction of these assumptions (i.e., sufficient conditions), a gradient-based algorithm will always achieve the maximum value of the cost functional starting from any initial field [11,14,15]. Under the same assumptions, analogous studies of the landscape for J_O and J_W show a similar favorable topology including non-trapping saddle features at particular intermediate elevations on these landscapes. In addition, the *structure* of the control landscape, which refers to features other than the critical points, can play an important role in determining the efficiency of an algorithm (e.g., a local gradient procedure) for climbing the landscape. A highly complex landscape structure could force the algorithmically guided trajectory to take a circuitous path up the landscape (and through control space), making optimally controlling quantum systems a demanding task. However, recent studies using the gradient algorithm found that the landscape structure is very simple as manifested by R values near 1.0 [17–19], where $R = d_{\mathrm{PL}}/d_{\mathrm{EL}}$ $(\geqslant)1$ is the ratio of a control trajectory's path length d_{PL} to the Euclidean distance between its endpoints, d_{EL}, respectively, defined as

$$d_{\mathrm{PL}} = \int_0^{s_{\max}} \left[\frac{1}{T} \int_0^T \left(\frac{\partial E(s,t)}{\partial s} \right)^2 dt \right]^{\frac{1}{2}} ds \qquad (3)$$

and

$$d_{\mathrm{EL}} = \left[\frac{1}{T} \int_0^T [E(s_{\max},t) - E(0,t)]^2 dt \right]^{\frac{1}{2}}. \qquad (4)$$

For a state-to-state transition probability control landscape [18], as well as for quantum ensemble and unitary control landscapes [19], it was found that R generally took on values less than 2.0 for *gradient-guided* control trajectories, starting from the bottom and ending at the top of the landscape (i.e., the notions of "bottom" and "top," respectively, refer to the worst and best values of J, according to the application). Indeed, control trajectories were even found for which $R - 1 \sim 10^{-3}$ in some cases. Thus, these works reveal that quantum control landscapes admit a preponderance of nearly straight gradient-based monotonic trajectories (here, monotonicity is assured by the gradient algorithm) when going from the bottom to the top.

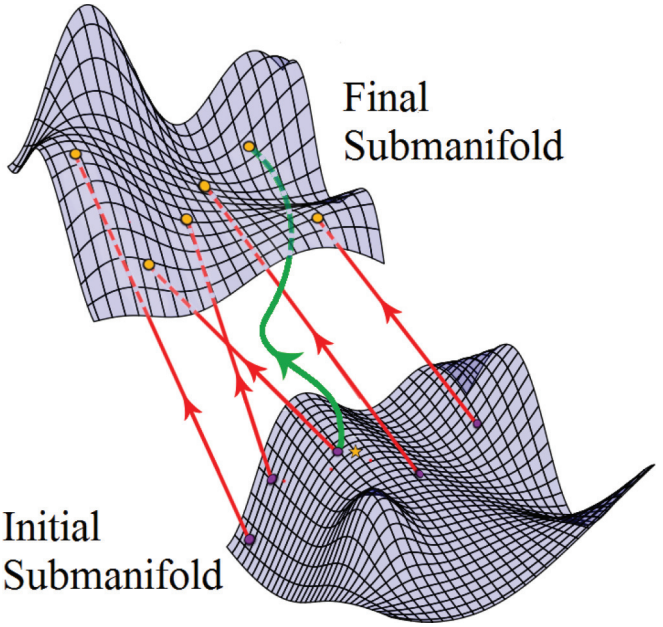

FIG. 1. Schematic showing portions of the initial and final submanifolds of fields, $\{E_I(t)\}$ and $\{E_F(t)\}$, respectively, in control space corresponding to a high final yield and a low initial yield. The specification of an initial or final yield J depends on the physical situation, as explained in the text. Straight paths in control space are displayed in red, connecting pairs of randomly selected points on the initial and final submanifolds. A gradient path, in green, originates at the same point as one of the monotonic straight paths (shown by the yellow star on the initial submanifold) but veers away, ending at a significantly different final control field on the final submanifold. The functional J always changes monotonically along a gradient path, but in general these paths are not straight. In contrast, along the exactly straight paths from the bottom to the top, J is observed generally to exhibit nearly, if not fully, monotonic behavior.

In this work, we further explore landscape structure by putting aside the gradient algorithm and its assured monotonicity of J and consider the converse situation of following exactly straight trajectories through control space with $R = 1.0$, while then assessing the degree to which J changes monotonically. In this situation, if we find exactly straight control trajectories also being frequently accompanied by monotonicity (or even near monotonicity) of J, then this occurrence would further demonstrate the presence of very smooth and simple landscape structural features. Performing this assessment is facilitated by prior control landscape analyses revealing the existence of submanifolds of controls at the bottom or top of the landscape [14,15]. Figure 1 depicts portions of these two critical submanifolds in control space and shows a curved trajectory (thick green curve) created by a gradient algorithm resulting in $R > 1$, while monotonically climbing the landscape. Also shown in Fig. 1 are straight trajectories (red lines), all satisfying $R = 1$, in control space connecting arbitrary points on the bottom and top submanifolds, thereby linking the lowest and highest values on the landscape. By examining large collections of randomly chosen straight paths among the bottom, top, and intermediate control

submanifolds associated with quantum control landscapes, we show that a plurality of these paths produces monotonically increasing values of J. One may liken this approach to assessing landscape smoothness as akin to taking a helicopter ride over the Rocky Mountains, while flying along a straight level path, and observing the height of the mountains directly below on the excursion. Naturally, the observer on such an trip would generally report terrain of repeatedly rising and falling height encountered along the ride. Similarly, the expectation is that following an analogous straight "flight" (path) through control space would encounter extended rising and falling J values on the way from the bottom to the top of the landscape. Expressed in such terms, our observation in Sec. III of only relatively few lapses of monotonicity in most cases, and modest variation from monotonicity in the remaining cases, bolsters the evidence for the existence of an unexpectedly simple quantum-control-landscape structure. This finding does not, in and of itself, provide a simple constructive "straight-shot" control algorithm, as the results in this paper rest on the exploitation of prior identification of the controls with J values corresponding to the bottom and top of the landscape. However, our findings suggest that an efficient algorithm may exist, specifically honed for quantum control, which can exploit the generally smooth nature of control landscapes. The present paper lays the foundation for future research along this line.

The remainder of the paper is organized as follows. Section II explains how the randomly chosen straight control paths are constructed, and Section III furnishes illustrations of the landscape behavior upon following such paths. Section IV contains a discussion and conclusions. Finally, the Appendix presents a statistical argument to explain the observed smooth features of the landscapes which arise when many interfering pathways contribute to the control mechanism involved.

II. STRAIGHT FIELD PATHS

The trajectories we consider in this work are straight paths in control space, where each path begins at a field $E_I(t)$ producing a low (or poor) initial value of the cost function $J_{if} = P_{i\to f}$ on the landscape and ends at a final field $E_F(t)$ producing a corresponding high (or good) value of J_{if}. These paths are parameterized by a variable $0 \leqslant v \leqslant 1$ (i.e., equivalent to s discussed above but referred to as v here to distinguish the exactly straight paths from the gradient-guided trajectories), so that each path is defined by

$$E(v,t) = (1-v)E_I(t) + vE_F(t), \tag{5}$$

where $J[E_I(\cdot)] = J^I$ and $J[E_F(\cdot)] = J^F$. We also consider analogous cases for trajectories between critical points (including the bottom and top) for J_O and J_W; a critical point is where the first derivative of the landscape cost function, with respect to the field, is 0. To generate a straight trajectory, we first choose two random control fields, $E_1(0,t)$ and $E_2(0,t)$, and use D-MORPH to continuously adjust each field until they, respectively, reach $J[E_1(s_{\max_1},t)] = J^I$ and $J[E_2(s_{\max_2},t)] = J^F$, where $s_{\max_i}$ is the appropriate final value of s in each case needed to reach either J^I or J^F, respectively. We then set $E_I(t) = E_1(s_{\max_1},t)$ and $E_F(t) = E_2(s_{\max_2},t)$ for use in Eq. (5), and the process is repeated many times to create a family of controls lying as a set of points on the bottom and top submanifolds (or specified critical points for J_O and J_W). There is no special relationship between field $E_I(t)$ and field $E_F(t)$, as they are all randomly chosen as pairs from the two respective manifolds. Each of the random fields is constructed starting with

$$E(t) = \frac{1}{F_0}\exp[-0.3(t-T/2)^2]\sum_{n=1}^{M} a_n \sin(\omega_n t + \phi_n), \tag{6}$$

where $T = 10$, and the amplitudes a_n and phases ϕ_n are chosen randomly from the uniform distributions $[0,1]$ and $[0,2\pi]$, respectively. M is set to 20, with the frequencies being $\omega_n = n$, so that the initial control field contains frequencies that coincide with every transition in the systems given by H_0 in Eqs. (7) and (11). The normalization factor F_0 is set for each random field to ensure that it has unit fluence. Each initial field chosen in Eq. (6) is then directed by the D-MORPH algorithm to go either to the bottom submanifold or the top submanifold. This process was performed by discretizing the initial random field in Eq. (6) into 10^4 time points, with the field strength at these points being the control variables used by D-MORPH and in subsequent straight paths through control space using Eq. (5). Typically, 500 field pairs corresponding to points on the initial and final critical submanifolds were found. Arbitrary units are used in the simulations, and T is the final time at which J is evaluated.

III. RESULTS

A. State-to-state transition probability landscape

We now provide numerical illustrations probing the landscape structure revealed by following exactly straight field paths with Eq. (5). The state-to-state transition probability landscape in this work is associated with the Hamiltonian in Eq. (1), where

$$H_0 = \begin{pmatrix} -10 & 0 & 0 & 0 & 0 \\ 0 & -7 & 0 & 0 & 0 \\ 0 & 0 & -3 & 0 & 0 \\ 0 & 0 & 0 & 2 & 0 \\ 0 & 0 & 0 & 0 & 8 \end{pmatrix} \tag{7}$$

and

$$\mu = \begin{pmatrix} 0 & \pm 1 & \pm 0.5 & \pm 0.5^2 & \pm 0.5^3 \\ \pm 1 & 0 & \pm 1 & \pm 0.5 & \pm 0.5^2 \\ \pm 0.5 & \pm 1 & 0 & \pm 1 & \pm 0.5 \\ \pm 0.5^2 & \pm 0.5 & \pm 1 & 0 & \pm 1 \\ \pm 0.5^3 & \pm 0.5^2 & \pm 0.5 & \pm 1 & 0 \end{pmatrix}. \tag{8}$$

The signs of the dipole matrix elements were chosen randomly such that the matrix remained symmetric and then were fixed for all the simulations. We remark that the diagonal elements of Hamiltonian H_0 are rather arbitrarily chosen, and the falloff of the dipole coupling in μ is physically reasonable as the levels become further separated. Our extensive numerical studies revealed little impact on the landscape features for reasonable variations of H_0 and μ. Figure 2 displays the value of $P_{1\to 5}(v)$ on the landscape as a function of v in Eq. (5) for a collection of 500 random straight control-space paths that were constructed using the procedure set out in Sec. II. The paths

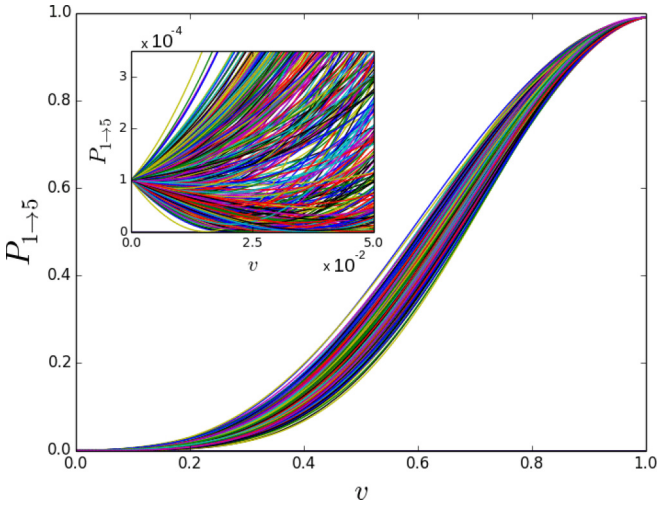

FIG. 2. The value of $P_{1\to5}$ along a collection of 500 straight paths between randomly chosen points $E(0,t) = E_I(t)$ on the submanifold close to the bottom of the landscape, such that $J[E(0,t)] = 10^{-4}$, and randomly chosen points $E(1,t) = E_F(t)$ on the submanifold close to the top of the landscape, such that $J[E(1,t)] = 0.99$. For a large portion of the paths, $P_{1\to5}(v)$ increases monotonically over $0 \leqslant v \leqslant 1$ as the path is traversed from the bottom to the top utilizing Eq. (5). Inset: Near the bottom of the landscape, for a subset of the straight control paths, the value of $P_{1\to5}$ initially decreases by a small amount near the beginning of the trajectory.

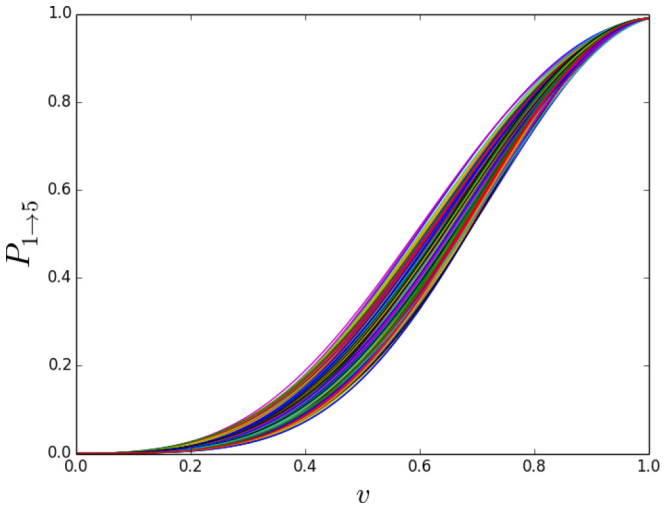

FIG. 3. The value of $P_{1\to5}$ for a collection of 500 straight control paths with each initial point located at $E(0,t) = E_I(t) = 0$, producing $P_{1\to5} \equiv 0$, and the final point being a randomly chosen field $E(1,t) = E_F(t)$ such that $P_{1\to5}[E(1,t)] = 0.99$. Each of these straight paths in control space results in a strictly monotonic climb of the transition probability $P_{1\to5}$ control landscape.

begin with initial fields $E(0,t)$ all producing $P^I_{1\to5} = 10^{-4}$, which approximates the bottom submanifold of the landscape, and terminate at a height of $P^F_{1\to5} = 0.99$, which is considered to be an acceptably high yield. Remarkably, the paths appear to be monotonic. However, the inset in Fig. 2 shows that approximately 45% of the trajectories initially proceed to lower values of $P_{1\to5} < 10^{-4}$; for this set of trajectories, these "dips" only occur in the beginning, at extremely low values on the landscape.

Since the nonmonotonic behavior in Fig. 2 occurs only near the initial submanifold where $P^I_{1\to5} = 10^{-4}$ on the landscape, it is natural to consider the outcome of changing the starting and ending values $P^I_{1\to5}$ and $P^F_{1\to5}$, respectively. We carried out simulations using similar values of $P^I_{1\to5}$ but very different values of $P^F_{1\to5}$ (data not shown), which revealed that the degree of monotonicity found along a straight control path is not affected by the choice of $P^F_{1\to5}$. However, it was found that starting at larger initial values of $P^I_{1\to5}$ resulted in deeper dips like those in the inset in Fig. 2. These collective results imply that we may specify the final submanifold corresponding to any desired high value of $P^F_{1\to5}$ and focus attention on taking the initial yield to its extreme limit of $P^I_{1\to5} = 0$.

As a step towards the latter limit, we performed additional simulations where $P^I_{1\to5}$ was further reduced (i.e., below 10^{-4} in Fig. 2), and as a result, fewer trajectories were found to exhibit nonmonotonic behavior (not shown here). Note that the climb down from randomly chosen suboptimal landscape levels at the initial value $s = 0$ to the near landscape bottom is very fast, indicative of the structure being smooth in the lower portion of the landscape. We then considered the extreme case of an initial field $E_I(0,t) = 0$, which produces $P^I_{1\to5} \equiv 0$, and collected 500 straight paths where each final field $E_F(t)$ corresponded to the value $P^F_{1\to5} = 0.99$. Utilizing these fields in Eq. (5) with $E_I(0,t) = 0$ produced the results shown in Fig. 3, where *all* of the straight field paths led to $P_{1\to5}(v)$ proceeding monotonically up the landscape (we have verified this behavior by checking for satisfaction of the inequality $\frac{dP_{1\to5}}{dv} = \int \frac{\delta P_{1\to5}}{\delta E}\frac{\partial E}{\partial v}dt > 0$ at fine steps in v for all of the paths). We note as well for this class of straight field paths that $E(v,t) = vE_F(t)$ is simply amplitude modulation, $0 \leqslant v \leqslant 1$, but with the field form $E_F(t)$ containing complex positive and negative features arising from the sum in Eq. (6). The results in Fig. 2, even with its small deviation from monotonicity, and Fig. 3, showing strict monotonicity, imply that the $P_{i\to f}$ landscape is very smooth.

B. Quantum ensemble control landscape

The bottom and top submanifolds are the only critical points in the $P_{i\to f}$ landscape. In contrast, the quantum ensemble control landscape J_O generally possesses intermediate saddle critical submanifolds [16]. Thus, we consider quantum ensemble control in order to determine the effect of these saddle submanifolds on the monotonicity of a landscape climb upon following straight field paths. We again utilize the Hamiltonian and dipole matrices of Eqs. (7) and (8) and specify the initial density matrix

$$\rho = \begin{pmatrix} \frac{1}{3} & 0 & 0 & 0 & 0 \\ 0 & \frac{1}{3} & 0 & 0 & 0 \\ 0 & 0 & \frac{1}{5} & 0 & 0 \\ 0 & 0 & 0 & \frac{1}{15} & 0 \\ 0 & 0 & 0 & 0 & \frac{1}{15} \end{pmatrix}, \tag{9}$$

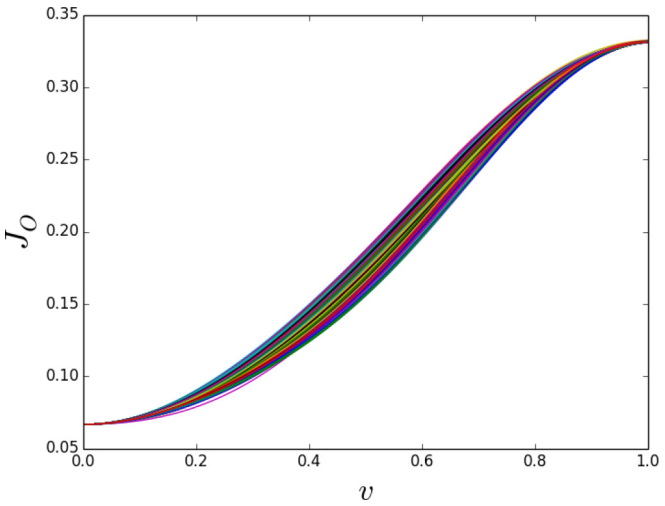

FIG. 4. The value of J_O along a collection of 500 straight control paths. The initial point in each path is a null field $E(0,t) = E_I(t)$ and the final point in each path is a randomly chosen field $E(1,t) = E_F(t)$ located at the top of the landscape. All of the straight paths monotonically climb to the top.

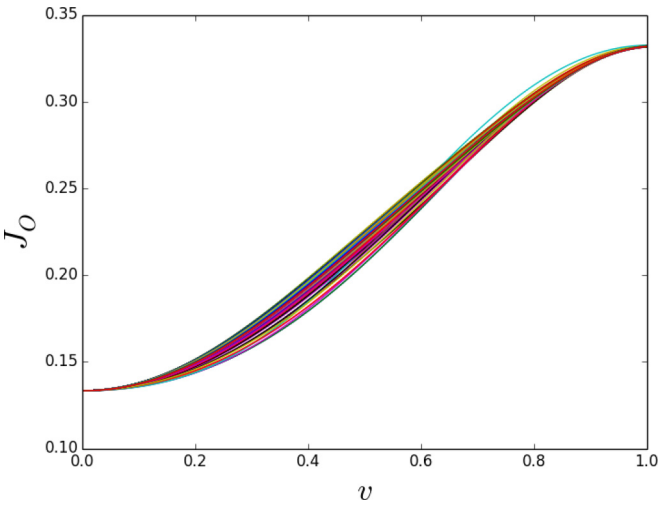

FIG. 5. The value of J_O along a collection of 500 straight control paths. Each path is driven by a field $E(v,t) = vE_F(t)$, where $E_F(t)$ is determined to produce a maximal yield [i.e., at $E(1,t) = E_F(t)$] by first starting with a random field and then optimizing it with D-MORPH. The field $E(0,t) = E_I(t) = 0$ gives a yield located on the saddle critical submanifold at $J_O = 2/15$. Importantly, all of the straight control paths correspondingly start at a saddle, and the trajectories all monotonically climb to the top.

with the observable

$$O = \begin{pmatrix} 0 & 0 & 0 & 0 & 0 \\ 0 & 0 & 0 & 0 & 0 \\ 0 & 0 & 0 & 0 & 0 \\ 0 & 0 & 0 & \frac{1}{2} & 0 \\ 0 & 0 & 0 & 0 & \frac{1}{2} \end{pmatrix}. \tag{10}$$

These matrices were chosen so that the null field $E_I(t) = 0$ corresponds to a point located at the bottom of the control landscape, where $J_O = \mathrm{Tr}(\rho O) = 1/15 \sim 0.0\overline{6}$. As in the previous section, we optimize J_O to the value $\frac{124}{375} \sim 0.331$ (the absolute maximum value is $\frac{1}{3}$) by starting with randomly chosen control fields in Eq. (6) to obtain 500 final fields $E_F(t)$. The observable value J_O along 500 straight paths between the null control field and the random final fields is plotted in Fig. 4. All of the paths show that J_O rises monotonically, indicating that the presence of intermediate critical submanifolds (at observable values of $J_O = 2/15$, $3/15$, and $4/15$) does not alter the conclusions in the previous section.

We also addressed the circumstances of taking straight field paths which correspond to beginning at an intermediate critical submanifold. This goal may be achieved by altering the order of the initial eigenvalues of ρ. In particular, we stipulate a new initial density matrix which arises from a permutation which swaps the third and last diagonal elements of ρ to form ρ'. With ρ' and $E_I(t) = 0$ the initial value of the ensemble observable is $J_O = \frac{2}{15}$, which is a saddle submanifold. In Fig. 5, we display J_O associated with 500 straight field paths of the form $E(v,t) = vE_F(t)$, where each final field $E_F(t)$ was determined by the procedure in Sec. II. All of the paths are again monotonic, thus suggesting that straight field paths to the top of the landscape need only begin on a critical submanifold to monotonically climb the landscape.

The final investigation pertains to whether straight field paths between two intermediate saddle submanifolds are also monotonic in the observable value J_O. To answer this, we altered ρ again in Eq. (9) with a permutation matrix which swaps the first and last diagonal elements of ρ to form ρ''. As a result, the final objective is to reach $J_O = \mathrm{Tr}(\rho'' O) = \frac{3}{15}$, which is a saddle submanifold. The initial state is again ρ' such that $J_O = \mathrm{Tr}(\rho' O) = \frac{2}{15}$ starts out as a saddle submanifold with $E_I(t) = 0$. The control fields are all of the form $E(t) = vE_F(t)$, where $E_F(t)$ is found using the procedure in Sec. II to reach the final saddle submanifold. In order to assure that $J_O = \frac{3}{15}$ is actually a saddle, the target cost was $\|\rho[E_F(t)] - \rho''\|$. Figure 6 displays J_O associated with 500 straight field paths between two saddle submanifolds. Not all of the paths are monontonic in J_O, so the results suggest that, for the quantum ensemble control landscape, if both endpoints of a straight field path correspondingly connect two intermediate saddle submanifolds, then J_O shows modest deviations from monotonicity.

C. Unitary transformation landscape

The unitary transformation landscape J_W also possesses intermediate saddle critical submanifolds [20]. We considered straight field paths for a unitary transformation landscape using the Hamiltonian and dipole matrices

$$H_0 = \begin{pmatrix} -10 & 0 & 0 & 0 & 0 & 0 \\ 0 & -7 & 0 & 0 & 0 & 0 \\ 0 & 0 & -3 & 0 & 0 & 0 \\ 0 & 0 & 0 & 2 & 0 & 0 \\ 0 & 0 & 0 & 0 & 8 & 0 \\ 0 & 0 & 0 & 0 & 0 & 15 \end{pmatrix} \tag{11}$$

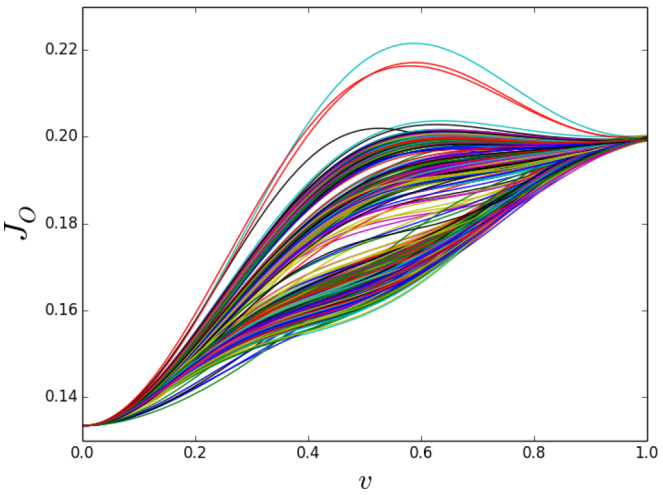

FIG. 6. The value of J_O along a collection of 500 straight control paths. The initial point in each path is a randomly chosen field $E(0,t) = E_I(t)$ located on the saddle critical submanifold at $J_O = 2/15$, and the final point in each path is a field $E(1,t) = E_F(t)$ located at the saddle critical submanifold with $J_O = 3/15$. Here not all of the straight control paths are monotonic in the cost function but the deviations from monotonicity reveal a gentle landscape free of gnarled features.

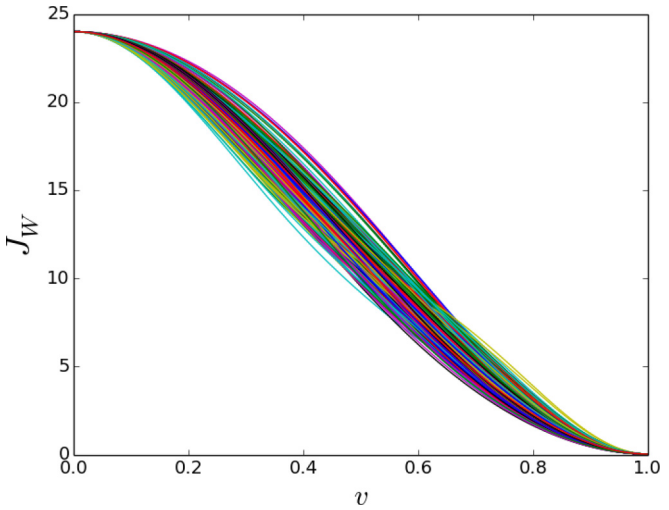

FIG. 7. The value of J_W along a collection of 500 straight control paths, with the initial point in each path located at a randomly chosen field $E(0,t) = E_I(t)$ yielding a unitary evolution operator $U = -W$ and the final points located at a randomly chosen field $E(1,t) = E_F(t)$ yielding an evolution operator $U = W$. Each straight control path interpolates between fields at the bottom and top of the unitary transformation landscape according to Eq. (5), and the landscape trajectory displays monotonic behavior, with no sign of being influenced by the intermediate saddle submanifolds of the landscape.

and

$$\mu = \begin{pmatrix} 0 & \pm 1 & \pm 0.5 & \pm 0.5^2 & \pm 0.5^3 & \pm 0.5^4 \\ \pm 1 & 0 & \pm 1 & \pm 0.5 & \pm 0.5^2 & \pm 0.5^3 \\ \pm 0.5 & \pm 1 & 0 & \pm 1 & \pm 0.5 & \pm 0.5^2 \\ \pm 0.5^2 & \pm 0.5 & \pm 1 & 0 & \pm 1 & \pm 0.5 \\ \pm 0.5^3 & \pm 0.5^2 & \pm 0.5 & \pm 1 & 0 & \pm 1 \end{pmatrix}. \tag{12}$$

For $J_W = \|W - U(T)\|^2$ the worst field will produce the transformation $U(T) = -W$ such that $J_W = 4N = 24$ in the present circumstance with $N = 6$. The choice for W was picked as $W = -U_I(T)$, where $U_I(T)$ was generated from a random field $E_I(t)$ of the form in Eq. (6). A set of 500 optimal fields $E_F(t)$ was generated by the procedure in Sec. II, seeking the final cost $J_W[E_F(t)] = 0.01 \times 4N = 0.24$. Straight trajectories through control space were then generated by Eq. (5). The associated values of J_W along these straight control paths are shown in Fig. 7. As in Fig. 3, all of the straight field paths produce monotonic trajectories $J_W(v)$ and show no hint of being influenced by saddle submanifolds occurring at values of $J_W = 4$, 8, 12, and 16.

By finding a suitable initial field $E_I(t)$ such that the straight field path begins at a saddle submanifold, we can further inquire whether straight trajectories beginning at a saddle point and ending at the bottom of the landscape (the optimal value taken here is $0.01 \times 4N = 0.24$) are also monotonic in J_W. By specifying $W = U_I(T) * X$, where $U_I(T)$ is defined as in the preceding paragraph, as being generated from the random field $E_I(t)$ and $X = \mathrm{diag}(-1,-1,+1,+1,+1,+1)$, we ensure that the randomly selected field $E_I(t)$ lies on a saddle point [20] with

$$J_W = 2N - 2\mathrm{Re}\{\mathrm{Tr}\,(XU_I^\dagger(T)U_I(T))\} = 8.$$

Figure 8 displays J_W along 500 straight field paths beginning at this saddle submanifold with the field $E_I(t)$ and ending near the optimal value of the landscape following the procedure in Sec. II to generate the optimal fields $E_F(t)$. All of the trajectories on the landscapes are still monotonic in J_W. Finally, we assessed whether straight field paths between two saddle submanifolds also produce monotonic paths for $J_W(v)$.

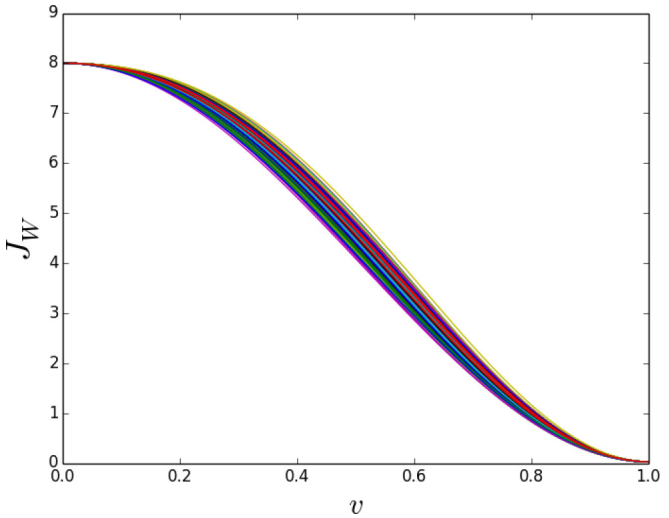

FIG. 8. The value of J_W along a collection of 500 straight control paths. Each path begins at a random field $E(0,t) = E_I(t)$ located on a saddle point where $J_W = 8$ and ends at a random field $E(1,t) = E_F(t)$ located at the bottom of the unitary transformation landscape. All of the runs are monotonic.

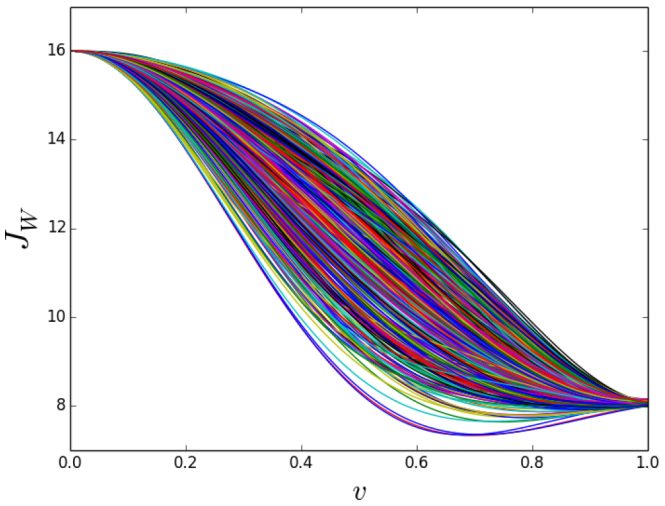

FIG. 9. The value of J_W along a collection of 500 straight control paths, with the initial point in each path located at a randomly chosen field $E(0,t) = E_I(t)$ on a saddle point with $J_W = 16$ and the final points located at a randomly chosen field $E(1,t) = E_F(t)$ also located on a saddle point, with $J_W = 8$. A small subset of the paths displays nonmonotonic behavior of the cost function consistent with encountering only modest landscape structural features.

In this case, after choosing the random initial field $E_I(t)$, we specify $W = U_I(T) * Y$, where $U_I(T)$ is generated from $E_I(t)$ as described above and $Y = \mathrm{diag}(-1,-1,-1,-1,+1,+1)$. As a result, the initial field $E_I(t)$ lies on a saddle submanifold with

$$J_W = 2N - 2\mathrm{Re}\{\mathrm{Tr}\,(Y U_I^\dagger(T) U_I(T))\} = 16.$$

Then, we generate a set of 500 optimal fields $E_F(t)$ by starting with random fields according to Eq. (6) and seeking to minimize the modified cost function $J'_W = \|W * Y * X - U(T)\|^2$, where X is defined as in the previous paragraph. As a result, the final fields $E_F(t)$ lie on a saddle submanifold with

$$J_W = 2N - 2\mathrm{Re}\{\mathrm{Tr}\,(XYY U_I^\dagger(T) U_I(T))\} = 8.$$

In Fig. 9, we plot J_W along 500 straight paths between these two saddle submanifolds. Although a preponderance of the paths is monotonic, there are clearly several which fall below the initial value of $J_W = 8$. It is noted that the results in Figs. 7–9 each correspond to assessing features in a statistically chosen family of landscapes, as distinct values of W were generated for each trajectory.

IV. DISCUSSION AND CONCLUSIONS

This paper shows that nearly all the exactly straight paths in control space taking the yield from close to the bottom of the landscape to the top correspond to monotonically increasing climbs. Furthermore, when critical saddle submanifolds exist and can be exactly accessed, straight paths in control space between saddle generating fields and the top are still monotonic in the yield and are not influenced by the other critical submanifolds. However, it was found that straight paths between fields starting and fields ending at saddles showed a preponderance of monotonic behavior, along with some modest deviations. Even the trajectories showing the highest degree of nonmonotonic behavior reflect merely gentle landscape features (i.e., typically at most a single small dip or rise deviation from monotonicity was present in these cases, as shown in Figs. 6 and 9). These findings appear surprising, as the quantum control landscape is defined over a high-dimensional control space and encapsulates a generally very nonlinear relationship between the control field and the cost function. The collective observations from the simulations in this work bolster prior studies showing that paths taken up the landscape guided by a gradient algorithm (and thus guaranteed to be monotonic in the objective value) correspond to nearly straight trajectories through control space giving R close to 1.0 [17–19]. The present work gives a complementary perspective on landscape structure by following exactly straight control-field trajectories and then finding that the objective value was almost always monotonic if the trajectories connected critical submanifolds including the bottom and top of the landscape. These dual perspectives are both reflective of the existence of a dramatically simple landscape structure. The Appendix establishes a statistical basis to understand the observed general smoothness of the landscape by considering the multiple interfering pathways that often arise in reaching the desired objective. In this regard, the analysis performed in the Appendix for $P_{i\to f}$ and $\mathrm{Tr}\,(\rho O)$ is distinct from considering $\|W - U\|^2$, but the conclusion in all cases is to generally expect monotonic variation of the objective upon taking a straight path in control space. The analysis involved is statistical, and as such some deviation from monotonicity could still occur, as found in the simulations.

We remark again that all the studies in this work started and ended at submanifolds of critical points. Each manifold is inherently flat with a countable number of steepest paths up (or down, as appropriate) accompanied by an-infinite dimensional flat null space. In this regard, we note the finding with the transition probability landscape in Sec. III A, where starting farther from the bottom of the landscape leads to deeper dips before continuing on a final monotonic climb. Thus, we performed a further numerical study of landscape structure based on taking straight shots between arbitrary initial and final fields for all of the landscapes J_{if}, J_O, and J_W. We observed that straight paths between fields chosen randomly from arbitrary locations on any of the landscapes showed only modest degrees of nonmonotonic behavior, again consistent with the landscapes being remarkably free of gnarled structures.

The emerging picture of a very smooth control landscape structure suggests seeking an efficient climbing algorithm which is able to discover straight paths through control space while attaining at least near monotonicity of the yield while climbing. In this regard, it is significant to note that the submanifold at the top of the landscape has vanishing measure in an infinite-dimension control space, so it would seem that picking an initially fixed direction to proceed along in control space would rarely, if ever, yield a monotonic path to the top or even arrive close to it. However, the results in this work show that such desirable directions exist. The challenge is to find a *constructive* algorithm that does not utilize prior knowledge of fields on the top submanifold to identify those initial directions. In creating such an algorithm, the straight

nature of a control path arriving at the top of the landscape appears to be a more desirable characteristic than monotonicity of the yield, as straight control paths are likely to be shorter and require fewer evaluations of the cost functional. In this context, the evidence shows [17–19] that the gradient algorithm is already very good, as all runs generally achieve $R < 2.0$, but the gradient algorithm still appears to be wanting in terms of reaching the desired ideal efficiency, given the evidently generic simple structure of quantum control landscapes. We leave open for future work consideration of the possibility of creating a constructive algorithm for climbing the landscape by progressing in a straight line in control space.

As a concluding remark we return to the prior analyses of generally finding very favorable control landscape topology based on what appears to be easily satisfied assumptions [11,14,15]. We now also see that the landscape structure rarely shows any significant gnarled structure. The dual very attractive landscape features of topology and structure, although apparently each of distinct physical origin, act in a cooperative fashion to provide a basis to generally expect ready discovery of effective control fields.

ACKNOWLEDGMENTS

A.N. acknowledges support from the US Army Research Office under Grant No. W911NF-13-1-0237, T.-S.H. acknowledges support from the US Army Research Office MURI under Grant No. W911NF-11-1-2068, and H.R. acknowledges partial support from the Templeton Foundation and the US National Science Foundation under Grant No. CHE-1058644.

APPENDIX: UNDERSTANDING THE BASIS FOR THE OBSERVATION OF GENERALLY STRUCTURE FREE QUANTUM CONTROL LANDSCAPES

1. Background

As discussed in the text, an experimental study [17] and a number of simulations [18,19,21] guided by the gradient algorithm revealed that the observed path length ratio R is generally low, $R \lesssim 2$, for climbing various types of quantum control landscapes. The simulations included either fields or Hamiltonian time-independent structural variables as controls. These studies considered either $P_{i\to f}$, $\mathrm{Tr}(\rho O)$, or $\|W-U\|^2$ as the objectives for optimization, in each case on the landscape denoted J. The overall finding that $R \lesssim 2$ implies that quantum control landscapes appear to be nearly devoid of structural features upon using a gradient algorithm to guide the optimization process. The present paper bolsters this finding by putting aside the gradient algorithm and, instead, following straight-shot paths through control space from an initial to a final field accompanied by an observation of the evolving value of the landscape height along a climb. The key finding in this paper is that almost all such trajectories are monotonic, again reflecting the presence of a simple landscape structure.

This Appendix lays out a foundation for understanding the collective observations about landscape structure summarized above. Importantly, the explanation has a generic character, in keeping with the observed simplicity of the structural findings found over a wide set of circumstances. Interestingly, the explanation of the landscape topological features also rests on generic theoretical foundations, but the structural analog has a distinct explanation linked to the nature of quantum control mechanisms possibly containing large numbers of significant participating interfering terms in the Dyson expansion of the unitary transformation driving a particular control objective. This definition of control mechanism expressed through the Dyson expansion [22] has proved to be useful in many simulations, and it also may be experimentally implemented [23]. The technical details of how to extract the relevant Dyson expansion terms are not important for understanding their linkage to explaining the general finding of small values for the path length ratio R.

Appendix 2 below lays out the Dyson expansion in a form particularly relevant to the pathway analysis, and Appendix 3 considers the expected behavior of $R(v)$, where $0 \leqslant v \leqslant 1$ is the progress variable along a straight-line field trajectory specified in Eq. (5) of the text. Appendix 3 considers the behavior of $R(v)$ in a separate fashion for the individual cases of $P_{i\to f}$, $\mathrm{Tr}(\rho O)$, and $\|W-U\|$. Some concluding remarks aree given in Appendix 4.

2. Quantum control mechanism viewed from the significant terms in the Dyson expansion

The Schrödinger equation for all applications considered in this paper may be written as follows by combining Eqs. (1), (2), and (5) of the text:

$$i\hbar\frac{\partial U(t)}{\partial t} = [(H_0 - \mu E_I(t)) - v\mu(E_F(t) - E_I(t))]U(t), \tag{A1}$$

where it is understood that $U(t) \equiv U(t,0)$. Various cases are considered in the text, including $E_I(t) = 0$, but the analysis here considers the general form in Eq. (5) that is re-expressed in the Hamiltonian on the right-hand side of Eq. (A1). In the cases of J being either $P_{i\to f}$ or $\mathrm{Tr}(\rho O)$, in the text we considered that J was being maximized, with $E_I(t)$ giving a lower yield than $E_F(t)$. If the opposite circumstance was of interest, then the operator on the right-hand side of Eq. (A1) needs to be equivalently written as

$$[(H_0 - \mu E_F(t)) - (v-1)\mu(E_I(t) - E_F(t))]. \tag{A2}$$

In this case the derivations in Appendixes 3 a and 3 b below follow in the same way, with the conclusions being that monotonic minimization is expected. In the case of $J = \|W-U\|^2$ in the text and Appendix 3 c below we naturally start at a higher critical point on the landscape, seeking to be at a final lower one. If, once again, the opposite circumstance was sought, then the Hamiltonian form in Eq. (A2) applies, with the result on the monotonicity being more complex to assess. However, in all practical physical circumstances the goal is to minimize $J = \|W-U\|^2$, and the analysis as presented is consistent with the general findings in the simulations.

For notational simplicity, we make the definitions $H_0'(t) = H_0 - \mu E_I(t)$ and $\Delta E(t) = E_F(t) - E_I(t)$ to rewrite Eq. (A1) in the following form:

$$i\hbar\frac{\partial U(t)}{\partial t} = [H_0'(t) - v\mu\Delta E(t)]U(t). \tag{A3}$$

A new evolution operator is defined, $\mathcal{U}(t)$, where $U(t) = U_0(t)\mathcal{U}(t)$, permitting Eq. (A3) to be rewritten in the interaction

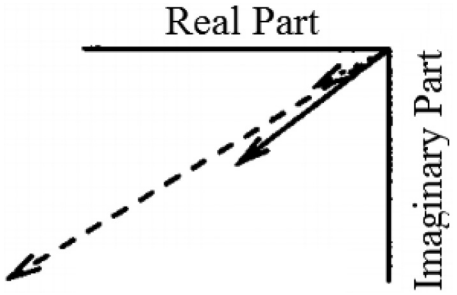

FIG. 10. The complex amplitudes entering into the Dyson expansion, Eq. (A5), for optimizing $P_{1\to 3}$ in a four-level system. The amplitudes have been slightly separated for visual clarity. Note that these amplitudes in the complex plane are referred to as "composite pathways," with each arrow likely arising from multiple distinct terms in the Dyson expnasion and, therefore, exhibiting more interference structure than is directly evident. [Reprinted with permission from Ref. [22]. Copyright (2003) by the American Physical Society.]

representation,

$$i\hbar\frac{\partial\mathcal{U}(t)}{\partial t} = -v\mu(t)\Delta E(t)\mathcal{U}(t), \tag{A4}$$

where $\mu(t) = U_0^\dagger(t)\mu U_0(t)$ with $i\hbar\frac{\partial U_0(t)}{\partial t} = H_0'(t)U_0(t)$. In standard fashion, the Schrödinger equation in Eq. (A4) may be iterated to form a Dyson expansion,

$$\mathcal{U}_{if}(T) \equiv \langle i|\mathcal{U}(T)|f\rangle = \sum_{n=0}^{\infty} v^n\mathcal{U}_{if}^n, \tag{A5}$$

where the states $|i\rangle$ and $|f\rangle$ may be eigenstates of H_0 or chosen in some other physically motivated fashion associated with the nature of the objective. The nth term in Eq. (A5) has the form

$$\mathcal{U}_{if}^n = \left(\frac{i}{\hbar}\right)^n\langle i|\int_0^T dt_n\mu(t_n)\Delta E(t_n)\int_0^{t_n} dt_{n-1}\mu(t_{n-1})\Delta E(t_{n-1})$$
$$\ldots\int_0^{t_2} dt_1\mu(t_1)\Delta E(t_1)|f\rangle. \tag{A6}$$

The landscape structural analysis in Appendix 3 c is based on the assumption that the control mechanism has a number of significant amplitudes $\mathcal{U}_{if}^n$ entering into Eq. (A5). A variety of studies have been carried out investigating this matter, with some evident trends in behavior. Two extreme limiting cases are shown in Figs. 10 and 11, respectively, corresponding to from a few constructively cooperating amplitudes $\mathcal{U}_{if}^n$ to a very large number of rather uniformly distributed amplitudes in the complex plane. Most cases studied lie between these extremes, but still with a significant number of amplitudes scattered in the complex plane.

A previous work examined the relation of the landscape structure to the mechanism based on the Dyson expansion [25]. Although no evident pattern was found in relating mechanism to structure, all of the cases considered in the study had at least modest number of significant terms in Eq. (A5). This Appendix takes a closer look at the relation of mechanism and landscape structure viewed through the Dyson expansion. The analysis assume that a significant number of terms contribute to Eq. (A5), leading to a particular approximation whose conclusion is consistent with the observed generally monotonic

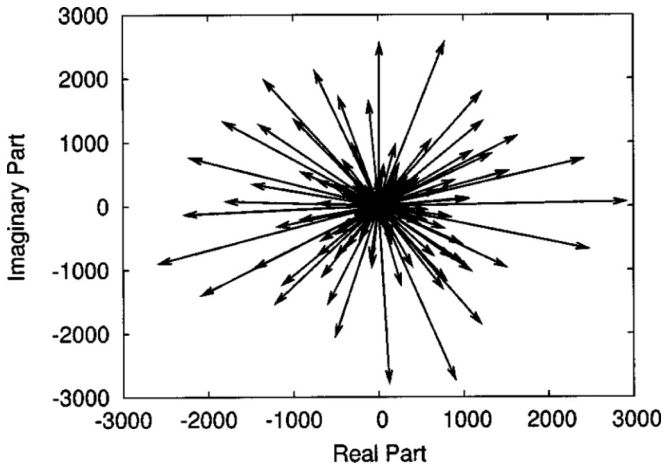

FIG. 11. The complex amplitudes of the Dyson expansion, Eq. (A5), are shown for an intense field eliciting many higher order multiphoton processes. In spite of the magnitude of the amplitudes, their combined sum is equal to 1.0 within computational precision. [Reprinted with permission from Ref. [24]. Copyright (2004), AIP Publishing LLC.]

climbs of the landscape. Although this conclusion explains the observed rather featureless structure of the landscape, the result rests on specified approximations, such that some exceptions to the conclusion may be expected to arise, as found in the numerical results in the text. Importantly, the exceptions to monotonicty still reveal a very modest landscape structure. Finally, the analysis below utilizes the interaction representation at the final time $U(T) = U_0(T)\mathcal{U}(T)$, which at most introduces a basis set change from the numerical studies in the text. This basis set change is not significant, as the target goals in the text were all chosen arbitrarily.

3. Landscape structure assessment

The assessment in this section separately considers the three cases of $P_{i\to f}$, $\mathrm{Tr}(\rho O)$, and $\|W - U\|^2$.

a. $P_{i\to f}, i \neq f$

We have that

$$P_{i\to f} = |\mathcal{U}_{if}|^2. \tag{A7}$$

It is convenient for our purposes here to rewrite Eq. (A5) as

$$\mathcal{U}_{if} = \delta_{if} + \sum_{n=1}^{\infty} v^n|\mathcal{U}_{if}^n|\exp\left(i\phi_{if}^n\right) \tag{A8}$$

$$= \sum_{n=1}^{\infty} v^n|\mathcal{U}_{if}^n|\exp\left(i\phi_{if}^n\right), \tag{A9}$$

where $\mathcal{U}_{if}^n = |\mathcal{U}_{if}^n|\exp(i\phi_{if}^n)$ and the last step is based on $i \neq f$. Combining Eqs. (A7) and (A9) gives

$$P_{i\to f} = \sum_{n=1}^{\infty}\sum_{n'=1}^{\infty} v^{n+n'}|\mathcal{U}_{if}^n||\mathcal{U}_{if}^{n'}|\exp\left[i\left(\phi_{if}^n - \phi_{if}^{n'}\right)\right]. \tag{A10}$$

Under the assumption that a significant number of terms enter into Eq. (A10), with $\{\exp(i\phi_{if}^n)\}$ rather uniformly spread over

2π radians in the complex plane, along with the moduli $\{|\mathcal{U}_{if}^n|\}$ being slowly varying with respect to n, we may make a random phase approximation in Eq. (A10) to arrive at

$$P_{i\to f} \simeq \sum_{n=1}^{\infty} v^{2n} \left|\mathcal{U}_{if}^n\right|^2. \tag{A11}$$

As we have v satisfying $0 \leqslant v \leqslant 1$, along with $|\mathcal{U}_{if}^n|^2$ being positive, it follows that the climb of the landscape should be monotonic, which is evident upon differentiating Eq. (A11) to produce

$$\frac{dP_{i\to f}}{dv} = \sum_{n=1}^{\infty} 2nv^{2n-1} \left|\mathcal{U}_{if}^n\right|^2 \geqslant 0. \tag{A12}$$

b. $J = \mathrm{Tr}(\rho(T)O)$

The objective, in the section title, may be rewritten as

$$J = \mathrm{Tr}\left[\mathcal{U}(T)\rho\mathcal{U}^\dagger(T)O\right], \tag{A13}$$

which becomes

$$J = \sum_{if} |\mathcal{U}_{if}|^2 \rho_i O_f. \tag{A14}$$

Here, ρ_i and O_f are the eigenvalues of the respective initial density matrix ρ and observable operator O with an appropriate basis $\{|i\rangle\}$ and $\{|f\rangle\}$ consistent with that circumstance. We may consider all of the eigenvalues of O as positive for convenience by adding an appropriate constant C to O as needed (i.e., this operation, if necessary, simply makes the shift $J \to J + C$). Upon substituting Eq. (A8) in Eq. (A14), we obtain

$$J = \sum_{if} \left|\delta_{if} + \sum_{n=1}^{\infty} v^n \left|\mathcal{U}_{if}^n\right| \exp\left(i\phi_{if}^n\right)\right|^2 \rho_i O_f \tag{A15}$$

$$= \sum_i \rho_i O_i + 2\sum_i \left(\sum_{n=1}^{\infty} v^n \left|\mathcal{U}_{ii}^n\right| \cos\left(\phi_{ii}^n\right)\right) \rho_i O_i \tag{A16}$$

$$+ \sum_{i,f} \sum_{n=1}^{\infty} \sum_{n'=1}^{\infty} v^{n+n'} \left|\mathcal{U}_{if}^n\right| \left|\mathcal{U}_{if}^{n'}\right| \exp\left[i\left(\phi_{if}^n - \phi_{if}^{n'}\right)\right] \rho_i O_f. \tag{A17}$$

Here, the lead term $\sum_i \rho_i O_i$ is just the initial value of J determined at $v = 0$. Upon making the same assumptions that were introduced regarding the behavior of the Dyson expansion in Appendix 3 a, we expect that the second term in Eq. (A15) may be neglected due to the cosine fluctuating rather uniformly over positive and negative values, finally resulting in the approximation

$$J \simeq \sum_i \rho_i O_i + \sum_{i,f} \sum_{n=1}^{\infty} v^{2n} \left|\mathcal{U}_{if}^n\right|^2 \rho_i O_f. \tag{A18}$$

Differentiation of this expression gives the result

$$\frac{\partial J}{\partial v} = \sum_{i,f} \sum_{n=1}^{\infty} 2nv^{2n-1} \left|\mathcal{U}_{if}^n\right|^2 \rho_i O_f \geqslant 0, \tag{A19}$$

which implies that we generally expect a monotonic climb of an observable landscape, as verified in numerical simulations in the text. The expression in Eq. (A19) also reduces to that of Eq. (A12) upon making a pure state transition with $\rho = |i\rangle\langle i|$ and $O = |f\rangle\langle f|, i \neq f$.

c. $J = \|W - U\|^2$

The objective in this section reduces to $J = 2N - 2\mathrm{ReTr}\,(W^\dagger U)$, and hereafter we neglect the constant $2N$. Thus the objective function becomes

$$J = -2\mathrm{Re} \sum_{i,f} (|W_{fi}^\dagger| |U_{if}) \exp(-i\chi_{fi}), \tag{A20}$$

where we have defined an element of the objective unitary transformation as $W_{fi}^\dagger = |W_{fi}^\dagger| \exp(-i\chi_{fi})$. Equation (A20) is assumed to be subject to minimization whether seeking W or some saddle as a target. In the present context, it is convenient to rewrite the expression in Eq. (A8) in the following form:

$$\mathcal{U}_{if} = \delta_{if} + \sum_{n=1}^{\infty} v^n \left|\mathcal{U}_{if}^n\right| \exp\left[i\left(\delta\phi_{if}^n + \chi_{fi}\right)\right]. \tag{A21}$$

Substitution of Eq. (A21) into Eq. (A20) results in

$$J = -2\sum_i |W_{ii}^\dagger| \cos(\chi_{ii}) - 2\sum_{i,f} |W_{fi}^\dagger| \sum_{n=1}^{\infty} v^n \left|\mathcal{U}_{if}^n\right| \cos\left(\delta\phi_{if}^n\right). \tag{A22}$$

Here we note that the first term in Eq. (22) is independent of v, and $\delta\phi_{if}^n$ is similarly independent of v. Thus, upon differentiation of Eq. (22), we obtain

$$\frac{\partial J}{\partial v} = -2\sum_{i,f} |W_{fi}^\dagger| \sum_{n=1}^{\infty} nv^{n-1} \left|\mathcal{U}_{if}^n\right| \cos\left(\delta\phi_{if}^n\right). \tag{A23}$$

The analysis of this case follows a different argument than those arising in Appendixes 3 a and 3 b. However, we expect that the phase $\delta\phi_{if}^n$ will likely satisfy $|\delta\phi_{if}^n| \ll 1$ for the case of $U \to W$ or approaching a saddle of J, as each of the elements of U must appropriately match those of W, which motivated the choice of $U_{if}^n = |\mathcal{U}_{if}^n| \exp[i(\delta_{if}^n + \chi_{fi})]$ in Eq. (A21). These arguments lead to the conclusion of expecting the approximate result $\frac{\partial J}{\partial v} \lesssim 0$ with $\cos(\delta\phi_{if}^n) > 0$ likely satisfied. Thus, we generally expect the trajectories of $J(v)$ to follow a monotonic path towards minimization of J, as overwhelmingly found in the simulations in the text.

4. General comments

In summary, the cases of $P_{i\to f}$ and $\mathrm{Tr}\,(\rho O)$, in Appendixes 3 a and 3 b, respectively, are expected to exhibit monotonic optimization behavior for sufficiently rich or multiterm control mechanisms. The case of $J = \|W - U\|^2$ in Appendix 3 c is analyzed on a different basis but still leading to the same conclusion of expecting monotonic minimization of the objective over the landscape. As all of the arguments involve approximations, exceptions could arise, but the evidence in the text shows that exceptions are rare.

[1] J. Werschnik and E. K. U. Gross, J. Phys. B: At. Mol. Opt. Phys. **40**, R175 (2007).
[2] D. Dong and I. R. Peterson, IET Control Theory Appl. **4**, 2651 (2010).
[3] C. Brif, R. Chakrabarti, and H. Rabitz, New J. Phys. **12**, 075008 (2010).
[4] R. Bücker, T. Berrada, S. van Frank, J. Schaff, T. Schumm, J. Schmiedmayer, G. Jäger, J. Grond, and U. Hohenester, J. Phys. B **46**, 104012 (2013).
[5] N. X. Truong, P. Hilse, S. Gode, A. Przystawik, T. Doppner, T. Fennel, T. Bornath, J. Tiggesbaumker, M. Schlanges, G. Gerber, and K. H. Meiwes-Broer, Phys. Rev. A **81**, 013201 (2010).
[6] S. Rosi, A. Bernard, N. Fabbri, L. Fallani, C. Fort, M. Inguscio, T. Calarco, and S. Montangero, Phys. Rev. A **88**, 021601(R) (2013).
[7] R. Hildner, D. Brinks, J. B. Nieder, R. J. Cogdell, and N. F. van Hulst, Science **340**, 1448 (2013).
[8] R. S. Judson and H. Rabitz, Phys. Rev. Lett. **68**, 1500 (1992).
[9] A. Weiner, Rev. Sci. Instrum. **71**, 1929 (2000).
[10] K. Moore, M. Hsieh, and H. Rabitz, J. Chem. Phys. **128**, 154117 (2008).
[11] R. Chakrabarti and H. Rabitz, Int. Rev. Phys. Chem. **26**, 671 (2007).
[12] M. A. Nielsen and I. L. Chuang, *Quantum Computation and Quantum Information* (Cambridge University Press, Cambridge, UK, 2004).
[13] A. Rothman, T.-S. Ho, and H. Rabitz, Phys. Rev. A **72**, 023416 (2005).
[14] H. Rabitz, M. Hsieh, and C. Rosenthal, Science **303**, 1998 (2004).
[15] H. Rabitz, T.-S. Ho, M. Hsieh, R. Kosut, and M. Demiralp, Phys. Rev. A **74**, 012721 (2006).
[16] T.-S. Ho and H. Rabitz, J. Photochem. Photobiol. A **180**, 226 (2006).
[17] J. Roslund and H. Rabitz, Phys. Rev. A **80**, 013408 (2009).
[18] A. Nanduri, A. Donovan, T.-S. Ho, and H. Rabitz, Phys. Rev. A **88**, 033425 (2013).
[19] A. Nanduri, O. M. Shir, A. Donovan, T.-S. Ho, and H. Rabitz, Phys. Chem. Chem. Phys. **17**, 334 (2015).
[20] H. Rabitz, M. Hsieh, and C. Rosenthal, Phys. Rev. A **72**, 052337 (2005).
[21] A. Donovan, V. Beltrani, and H. Rabitz, Phys. Chem. Chem. Phys. **13**, 7348 (2011).
[22] A. Mitra and H. Rabitz, Phys. Rev. A **67**, 033407 (2003).
[23] R. Rey-de-Castro, Z. Leghtas, and H. Rabitz, Phys. Rev. Lett. **110**, 223601 (2013).
[24] R. Sharp and H. Rabitz, J. Chem. Phys. **121**, 4516 (2004).
[25] A. Nanduri, A. Donovan, T.-S. Ho, and H. Rabitz, Phys. Rev. A **90**, 013406 (2014).